Deviation from the single-particle model in the angular distribution of thorium L_3 x rays in proton-impact ionization

T. Papp,* J. L. Campbell, and J. A. Maxwell
Guelph-Waterloo Program for Graduate Work in Physics, University of Guelph, Guelph, Ontario, Canada N1G 2W1
(Received 19 January 1993)

Angular distributions of L_3 x-ray transitions, including electric-dipole-forbidden ones, were measured for 1-, 2-, and 3-MeV proton impact on a thorium target, where the excitation and detection systems were cylindrically symmetric. A sophisticated spectrum-analysis technique was applied, where both the Lorentzian broadening of the transitions and the Si(Li) detector response function with various tailing features were taken into account. The anisotropy-parameter ratios are expected to be independent of the ionization process, and to be characteristic of the x-ray transitions in the independent-particle model. The ratios of the anisotropy parameters of the electric-dipole-allowed transitions were in disagreement with this expectation, even when the higher-order multipole contributions were taken into account. These results follow the same trend as earlier angular distribution and angular correlation measurements. Additionally, the electric-dipole-forbidden Lt (L_3M_2) and Ls (L_3M_3) transitions had a $P_4(\cos(\theta))$ term, which is not expected within the framework of the single-particle-model predictions. Possible causes for this discrepancy are explored.

PACS number(s): 32.30.Rj, 34.50.Fa, 32.80.Hd

I. INTRODUCTION

It is generally accepted [1,2] that there is good agreement between the theoretical and experimental radiative transition probabilities for atomic inner shells, although the scatter of the experimental data [3–5] is considerable. On the other hand, there are very few available experimental data on electric-dipole-forbidden transitions [1]. Usually the electric-dipole- ($E1$) forbidden transitions have small transition probabilities and are located close in energy to strong $E1$ allowed transitions, making them difficult to discern in x-ray spectra.

As is well known from nuclear physics, the angular distribution is sensitive to the multipolarity of the electromagnetic transition (e.g., electric L-pole, EL, and magnetic L-pole, ML). We used this technique earlier [6] to determine the $M2/E1$ mixing ratio for the $E1$ allowed Ll (L_3M_1) and $L\alpha_1$ (L_3M_5) transitions. The mixing ratios obtained were about 4 times larger for the Ll than those expected from theory [7]. However, it should be emphasized that, to describe the angular distribution of inner shell x-ray transitions, the so-called single-particle or independent-particle models are used [7,8]. Later we extended the study to include a wide range of target atoms and collected all the available experimental data for the anisotropy parameter ratios of the Ll and $L\alpha$ transitions [9]. Previously only the anisotropies of these two transitions have been reported, and almost all the experimental data were in disagreement with the theoretically expected values. Finding the reason for this disagreement may lead to an improvement of the theoretical model, or of the experimental technique, and to further this quest we decided to measure the angular distribution of the electric-dipole-forbidden transitions as well the $E1$-allowed transitions.

It was not clear that the required accuracy could be obtained by the experimental techniques presently available, as crystal diffraction spectrometers have drawbacks as regards both low efficiency and an inaccurately known polarization sensitivity of the crystal, while Si(Li) detectors have only moderate energy resolution; moreover in both cases the accuracy of the detector response functions needs to be considered. However, our present Si(Li) detector has one of the best resolutions available, and its response function was carefully determined earlier [10]; an earlier study on K-L coincidences with this detector has shown that the detector tailing did not change during two months of continuous operation [11]. We have found that the intensity and even the Lorentzian width of the $E1$-forbidden transitions can be determined by analyzing the spectra recorded with this detector [12]. In order to obtain large anisotropy, we chose proton impact for ionization and used a cylindrically symmetric detection system, thus reducing the number of parameters necessary to describe the angular distribution.

II. THEORETICAL BACKGROUND

The angular distribution of x-ray transitions for a cylindrically symmetric ionization and detection system can be found in many textbooks [13–16] and is expressed as

$$W(\theta)=\frac{1}{4\pi}\sum \hat{L}\hat{L}'\hat{a}\hat{a}'(-1)^{a+b+k+1}\frac{1+(-1)^{L+L'+\pi+\pi'+k}}{2}(L\,1L'-1|k0)\begin{Bmatrix}a' & L' & b\\ L & a & k\end{Bmatrix}\langle b\|L\|a\rangle\langle b\|L'\|a'\rangle \times\rho_{k0}(a,a')P_k(\cos\theta)\Delta\Omega\ , \quad (1)$$

where k=even. Here $W(\theta)$ denotes the photon intensity emitted into the $\Delta\Omega$ solid angle, $\hat{L}=\sqrt{2L+1}$, $(\,|\,)$ is a Clebsch-Gordan coefficient and $\{\,\}$ is a Wigner $6j$ coefficient, $\langle\,\|\,\|\,\rangle$ is the reduced matrix element, P_k is the kth-order Legendre polynomial, and $\rho_{k0}(a,a')$ is the density matrix, in the same notation as in Ref. [14]. There are only even k terms present, as a consequence of cylindrical symmetry and parity conservation. Equation (1) can be rewritten in the more usual, shorter form as

$$W(\theta)=W_0[1+\beta_k P_k(\cos\theta)]\Delta\Omega\ , \tag{2}$$

where k=even.

For independent ionization and decay processes, β can be expressed as

$$\beta_k=c\alpha_k A_k\ , \tag{3}$$

where A_k is proportional to the spherical components of the electric kth-pole tensor [13]. The correction factor c takes into account that L_3 holes can also be created indirectly by Coster-Kronig transitions [17], in which case the angular distribution is isotropic.

For the case of electric-dipole- ($E1$) allowed transitions the $\Delta(L=1,L'=1,k)$ triangle condition restricts the value of k to 0 and 2. The next strongest transition is the magnetic quadrupole ($M2$) transition, for which the interference term with the $E1$ is restricted by $\Delta(L=1,L'=2,k)$, with $k=0,2$. Although the $\Delta(L=2,L'=2,k)$ condition allows $k=0,2,4$ values, the $k=4$ term is proportional to the $M2$ transition probability, whose strength relative to the $E1$ transition is of the order of 10^{-4} [7] which is negligible for L and higher shells.

For $E1$-forbidden transitions the leading term is $E2$ and this obviously allows $k=0,2,4$ values. However, the $\Delta(a,a',k)$ triangle condition needs to be satisfied. The Hamiltonian of the ion should commute with the total angular momentum of the ionized atom, which corresponds to a and a'. In the theoretical calculations [7,8,18] it is customary to replace the total angular momentum with the angular momentum of the vacancy, which has the same angular momentum as the removed electron in the single-particle model. In the present case for the L_3 ($2p_{3/2}$) subshell the $a=a'=\frac{3}{2}$ value is used, assuming that this single-particle angular momentum has a well-defined value, or in other words that we are dealing with a pure angular momentum state [14]. This assumption introduces another restrictive condition, namely $\Delta(a=\frac{3}{2},a'=\frac{3}{2},k)$, which allows the $k=0,2$ values only. In the following we will assume the validity of this assumption; the lack (or presence) of the $P_4(\cos\theta)$ term in the experimental angular distribution may indicate the validity (or otherwise) of this assumption. Using a' values other than $\frac{3}{2}$ shows for instance that $a'=\frac{5}{2}$ with a 0.01 admixture would result in a measurable P_4 term in the angular distribution of the $E1$-forbidden transitions. It also shows that the signs of β_4 for the Lt (L_3M_2) and Ls (L_3M_3) transitions should be opposite.

Relativistic effects are important [19] and following [20] it can be easily shown that the strength of the small part of the L_3 electron Dirac wave function is around 30%–40% of the large part. Although the spherical part of the small component has a $d_{3/2}$ type wave function while the large component has a $p_{3/2}$ type wave function, for the description of the angular distribution only the total $j=\frac{3}{2}$ angular momentum will be important with the used approximation [21]. However, recent studies [22] show that the magnetic correlation energy is greater than the Coulomb one for medium and heavy atoms, which may affect the angular distribution of $E1$-forbidden transitions.

Following the assumption of the theoretical works [7,8], that the vacancy state, created by the ionization and filled during the observed electromagnetic transition, has a well-defined (pure) angular momentum, we have only one angular momentum value for each a and b state. Thus it is straightforward to obtain expressions for the α parameters. These were already reported for transitions where only two multipole components are present [16], but for completeness we rewrite them again

$$\begin{aligned}
&\alpha(Ll)=(0.5-\sqrt{3}\delta_1-0.5\delta_1^2)/(1+\delta_1^2)\ ,\\
&\alpha(L\alpha_2)=-0.4\ ,\\
&\alpha(L\alpha_1)=(0.1+\sqrt{7/5}\delta_1+0.3571\delta_1^2)/(1+\delta_1^2)\ ,
\end{aligned} \tag{4}$$

$$\alpha(Lt)=\frac{-0.5-\sqrt{3}\delta_2(M1/E2)+0.5\delta_2^2(M1/E2)}{1+\delta_2^2(M1/E2)}\ ,$$

$$\alpha(Ls)=\frac{1.549\delta_2(M1/E2)-0.4\delta_2^2(M1/E2)-1.265\delta_2(M3/E2)-0.6\delta_2^2(M3/E2)}{1+\delta_2^2(M1/E2)+\delta_2^2(M3/E2)}\ . \tag{5}$$

$\delta_L(ML'/EL)$ denotes the mixing ratio of the ML' and EL components for the marked transitions. Among the L_3-subshell x rays, the $L\alpha_2$ (L_3M_4) and $L\beta_{15}$ (L_3N_4) transitions have a special character, namely, that magnetic terms do not occur in their multipole expansions [4]. The ratio of the β anisotropy parameters of different x-ray transitions, having the same final states, does not depend on the alignment parameter and is dependent of the ionization process (as long as single ionization is the dominating ionization process). The ratio of the anisotropy parameters of these lines can be written as

$$\frac{\beta_2^{(1)}}{\beta_2^{(2)}}=\frac{\alpha^{(1)}cA_2}{\alpha^{(2)}cA_2}=\frac{\alpha^{(1)}}{\alpha^{(2)}}\ , \tag{6}$$

where the superscripts (1) and (2) refer to two different transitions.

The above ratios contain information about the decay process only, in the single-particle model, and provide the possibility to compare the experimental results with the theoretical calculation. These ratios depend sensitively on the angular momentum character of the participating atomic and photon states.

III. EXPERIMENT

A. Experimental setup

For angular distribution measurements it is desirable to use thin targets where the self-absorption correction is relatively small. In this case a high-efficiency detection technique is needed to observe the weak $E1$-forbidden transitions. This implies the use of Si(Li) detectors. The Link plc. Si(Li) detector (with resolution of 133 eV at 5.9 keV) whose response function was extensively studied earlier [10] was used to make these measurements. For the angular distribution measurement a thorium target was chosen since it is almost isotopically pure ^{232}Th with nuclear spin zero. It has a further advantage that the escape peak of the $L\alpha$ transition does not overlap with any electric-dipole-forbidden transition designated for study. The target was a 1-mg/cm^2-thick self-supporting metal foil. It was placed in the center of the scattering chamber described earlier [23], and is similar to those previously used by others [24,25]. The chamber, made of 1-cm-thick aluminum, is cylindrically symmetric around the axis perpendicular to the plane in which the detector is rotated, with an entrance hole window for the excitation beam. A 1-cm-wide horizontal slit window from 10° to 145° on one side and a window at 60° on the other side permit observation of the x rays. The slit and the window are covered with 0.050-mm-thick Mylar foil; the inner diameter of the chamber is 5 cm, and the inner surface of the chamber is covered by a 1-mm-thick carbon layer. The beam was collimated to 1 mm in diameter and had 2.5×10^{-3} rad angular divergence. The angular distributions were measured at 1-, 2-, 3-MeV proton projectile energy. The proton energy stability of this Van de Graaff accelerator is less than 0.3%, and during the course of the measurement the beam current fluctuated less than 10%.

Two Si(Li) detectors viewed the target. The principal detector, manufactured by Link plc., was placed on a turntable to take observations in the 22.5°–120° range. The second detector, manufactured by Ortec (resolution 180 eV at 5.9 keV) was used as a beam monitor detector. There were 3-cm air gaps between the detectors and the Mylar foil covering the slit and the window on the chamber. An additional 450-μm Mylar absorber was used in front of the Link detector to reduce the yields of the highly intense M x rays. The detector was collimated to 2 mm by a tantalum collimator to restrict the x rays to its central region, where the response function has very small low-energy tailing. A Nuclear Data 575 analog-to-digital converter equipped with an ND595 digital stabilizer recorded the spectra. The order of the observation angles was selected randomly, with each individual spectrum containing more than 10^6 counts in the Ll line. The count rate was 1500 counts per second for the 1-MeV protons and 2200 cps for the 2- and 3-MeV proton projectiles. Spectra were collected at ten angles for each proton energy, with about 5 h needed to collect each spectrum at these rates. A typical spectrum is shown in Fig. 1. A test measurement of 3-MeV proton impact on 20-μg/cm^2 Ni on a Mylar foil was performed, to check the geometrical alignment of the beam, target and the two detectors. The $K\alpha$,$K\beta$ spectra obtained by the two detectors were fitted and the ratio of the intensities detected by the movable detector were normalized to the one of the fixed detector. Both the $K\alpha$ ($\beta=0.0004\pm0.004$) radiation and the intensity ratio of $K\alpha$ and $K\beta$ radiation ($\beta=-0.006\pm0.005$) in the spectra of the movable detector were found to be isotropic as a function of the detection angle.

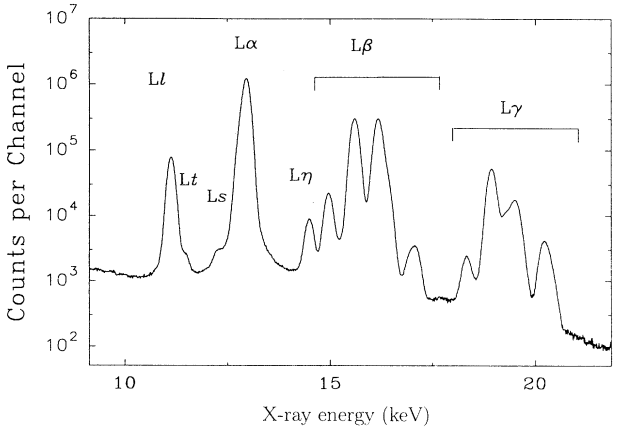

FIG. 1. L x-ray spectrum of thorium target bombarded by 1-MeV protons and measured with a Si(Li) detector at 60°.

B. Data evaluation

We have fitted the x-ray spectra in three energy ranges. The first range contained the Ll (L_3M_1), Lt (L_3M_2), Ls (L_3M_3) lines and the unresolved $L\alpha_{1,2}(L_3M_{4,5})$ doublet (Fig. 2). The second range covered part of the $L\alpha$ doublet, the $L\eta$ line, and the $L\beta$ group (Fig. 3), while the third range was limited to the $L\gamma$ group. In all ranges, a quadratic polynomial background was assumed. The response function of the detector (Link Series E) used here had been characterized earlier using monochromatic x rays [10]. The detector tailing was found to be very small above 10-keV energy where the L x rays of thorium occur. The same model was used for the detector response function as was reported earlier [10], viz., the sum of a Gaussian component and a low-energy tail component, the latter of which is constructed from an exponential tail, a long flat shelf extending to zero energy and a truncated flat shelf extending just beyond the silicon escape peak. Additionally we have the silicon es-

cape peak with a given intensity ratio to the photon peak. The photons were assumed to have a Lorentzian energy distribution for each x-ray transition, and this Lorentzian distribution was convoluted with the above-mentioned response function of the detector. The fitting computer code GPP [26] was used to perform the fit on a 80486 (33 MHz) personal computer, and the computer time needed for the analysis of a range of a spectrum was about an hour on average. At first we fitted the spectra using the tail parameters determined earlier [10]. However there were some small but noticeable remaining artifacts in the residuals of the spectra. To improve the quality of the fits, we summed the spectra measured at various angles for the same proton energy, and this very high statistics spectrum was fit with the tail parameters and Lorentzian widths left as variable parameters. An excellent fit was obtained, and these averaged tail parameters and Lorentzian widths were then used in the analysis of the individual spectra. The slight change in the tail parameters from the values previously recorded [10] is not surprising, since for instance ice build-up on the detector can effect the tail parameters on a long-time scale. We assumed that the average tail parameters were a good representation for the one-week measurement period as the detector bias was applied continuously from 2 weeks earlier and during the measurement. We did not expect any time variation in the detector response function over this short period; nevertheless, in order to minimize this possibility, the angles were selected in a random order, and the analysis indicated that indeed there was no time dependence noticeable in the results.

An excellent fit was obtained in the Ll,$L\alpha_{1,2}$ range where a reduced χ^2 value of 1.15 was obtained and only statistical fluctuations were observed in the residuals at the level from 15×10^6 to 20×10^6 events in the $L\alpha$ doublet. Because the $L\eta$ and the $L\beta_6$ lines sit on the upper Lorentzian tail of the $L\alpha$ peak it is important to include enough of the $L\alpha$ peak in the second fit region to model this tailing without including its own low-energy tailing which would substantially affect the low-energy tailing parameter values determined for the $L\eta$ and the $L\beta$ complex (as the low-energy tailing parameters are energy dependent). An average value of 5 was obtained for the reduced χ^2 in the second range, where the relative intensity ratio of the $L\beta_3$ and $L\beta_4$ lines was fixed at the theoretical intensity ratio [3] corrected for the detector efficiency and various absorptions. Similarly the intensity of those L_3 x-ray lines with energies greater than the $L\beta_{2,15}$ lines were correlated, and a single Lorentzian width was assumed for those lines. The $L\gamma$ peak complex was fit using Lorentzian broadened Gaussians for

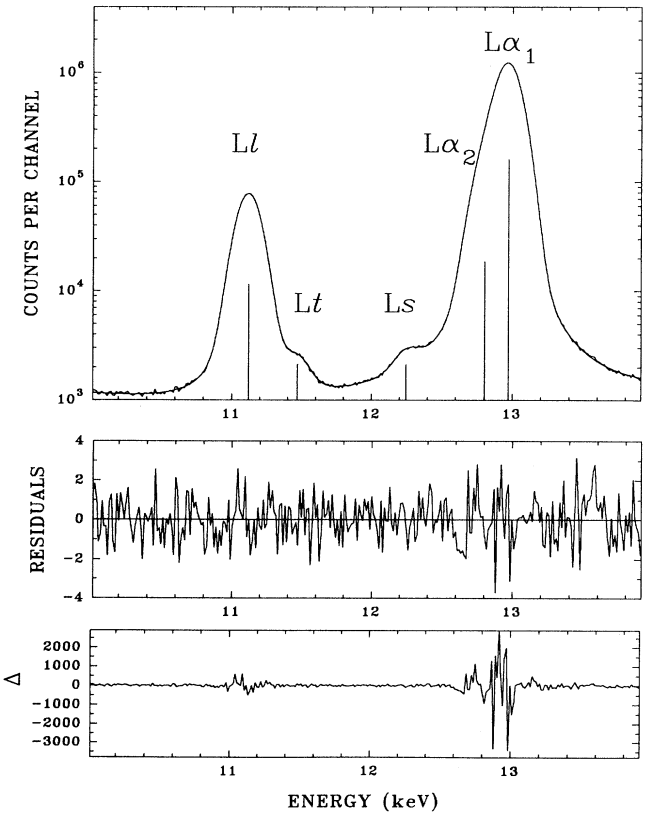

FIG. 2. Details of fit to the region of the thorium L x-ray spectrum containing the electric-dipole-allowed Ll and $L\alpha$ lines and the weak electric-dipole-forbidden Lt and Ls lines. The residues are in units of one standard deviation. Δ represents the difference between measured and fitted spectra.

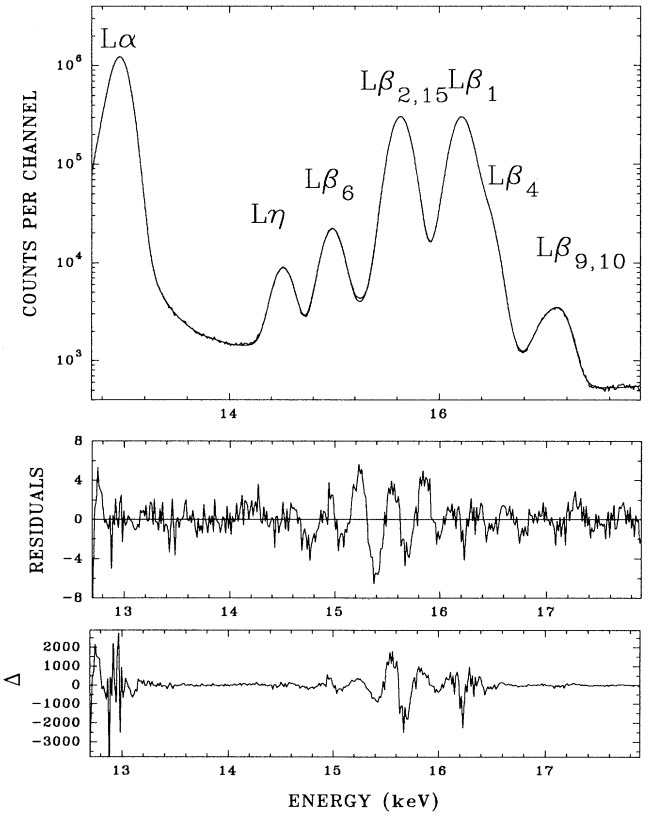

FIG. 3. Details of fit to the region of the thorium L x-ray spectrum containing the $L\eta$ line and the $L\beta$ group. The legends are the same as for Fig. 2.

the principal lines ($L\gamma_5$, $L\gamma_1$, $L\gamma_{2,3,6}$) and simple Gaussians for the weaker transitions. The Lorentzian widths used are presented in Table I.

After the fitting procedure, each of the line intensities was corrected for self-absorption. The line intensities in the $L\gamma$ group were summed and the resulting overall $L\gamma$ intensity was used later for normalization. For the 2-MeV proton case the $L\gamma$ yields were normalized to the monitor detector $L\alpha$ yields and were found to be isotropic as a function of the detector angle, which is in good agreement with earlier results [25] and with the theoretical expectation for single ionized atoms. Thus it is possible to employ the $L\gamma$ value as a normalization; using data obtained with one detector only has the advantage that any small change in the solid angle because of beam movement, or any dead-time effect in one or the other detector, does not affect the results. Also, since the self-absorption varies with angle, normalizing the line of interest to that of the $L\gamma$ group has the advantage that the self-absorption correction for the ratio is less than 2% at every angle for this target thickness. Any inaccuracy in the local thickness or the self-absorption correction will be negligible.

A sampling of the electric-dipole-allowed transitions angular distributions is shown in Fig. 4 with the line intensities normalized to that of the $L\gamma$ group. Our earlier studies [11,12] have shown that the separation of the $L\alpha$ doublet into $L\alpha_1$ and $L\alpha_2$ lines can be made using this Si(Li) detector and the fitting procedure described, provided that the spectrum has high statistics. Not only the expected intensity ratio but also the expected Lorentzian width were reproduced. The angular distribution measurement shows that this procedure gives reliable results, and as shown in Fig. 4, the angular distributions at every proton energy are well described by the expected second-order Legendre polynomial with the error bars from the fitting procedure consistent with the scatter of the data points. The intensity of the $L\alpha_1$ transition was divided by 12 to allow its presentation in the same figure.

The angular distributions obtained for the $E1$-forbidden Lt and Ls transitions are shown in Fig. 5(a) for

TABLE I. The Lorentzian widths of the L x-ray transitions of thorium used in the fits.

Transition	Widths (eV)
L_3M_1 (Ll)	25.5
L_3M_2 (Lt)	20.7
L_3M_3 (Ls)	20.7
L_3M_4 ($L\alpha_1$)	12.1
L_3M_5 ($L\alpha_2$)	11.8
L_2M_1 ($L\eta$)	26.7
L_3N_1 ($L\beta_6$)	33.7
$L_3N_{4,5}$ ($L\beta_{15,2}$)	20.1
L_1M_2 ($L\beta_4$)	24.2
L_1M_3 ($L\beta_3$)	24.2
L_2M_4 ($L\beta_1$)	11.0
$L_1M_{4,5}$ ($L\beta_{10,9}$)	14.6
L_2N_4 ($L\gamma_1$)	23.4
L_1N_2 ($L\gamma_2$)	32.9

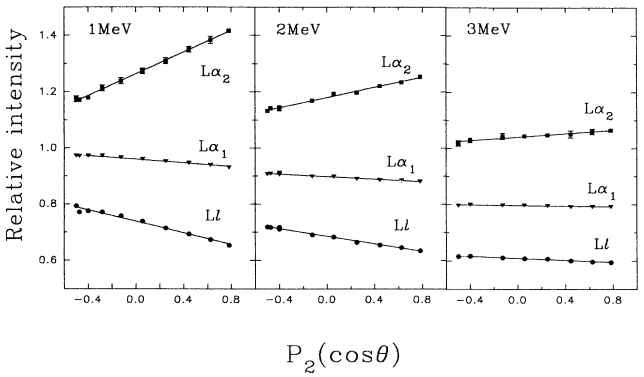

FIG. 4. Measured angular distributions for the Ll, $L\alpha_2$, and $L\alpha_1$ transitions of thorium bombarded by 1-, 2-, and 3-MeV protons as a function of the second-order Legendre polynomial. The intensity of each L x-ray line is expressed relative to the intensity of the $L\gamma$ group x rays. The intensity of the $L\alpha_1$ transition was divided by 12 to allow its presentation in the same figure.

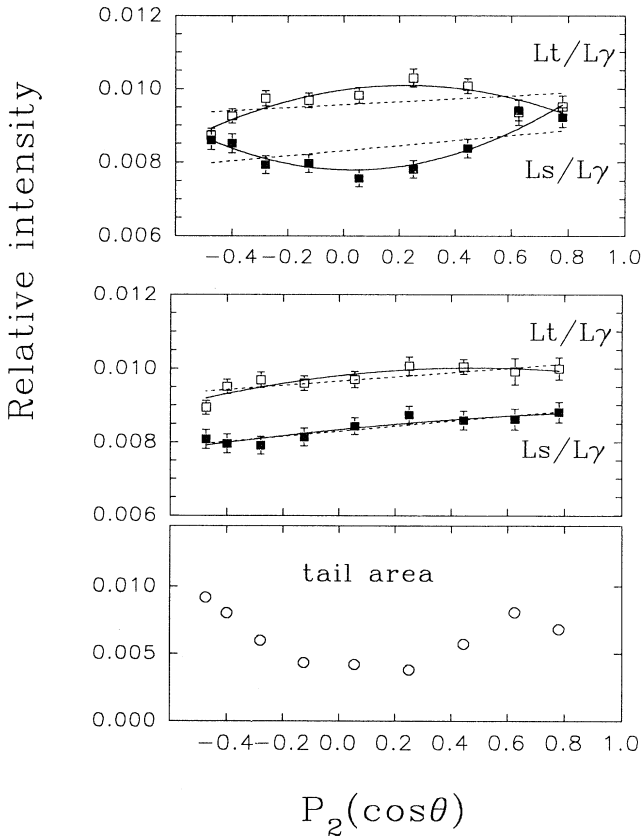

FIG. 5. Angular distribution of the dipole-forbidden Lt and Ls transitions of thorium ionized by 1-MeV protons, and normalized to the intensity of the $L\gamma$ group x rays. The upper part corresponds to the fit with averaged tail parameters (see text). The middle part represents the results of the fitting procedure with variable tail parameters. The lower part shows the tail area in the variable fit as a function of the second order Legendre polynomial. The dashed line and full curve are the best fits by the P_0+P_2 and the $P_0+P_2+P_4$ functions.

1-MeV proton impact. It is reiterated that the spectra were fitted using averaged tail parameters deduced from the sum spectrum over all angles. The unexpected feature is the deviation from linear behavior. The dashed lines represent the best fit by the function of zero- and second-order Legendre polynomial. The full curves represent the fit by the $P_0(\cos(\theta)) + P_2(\cos(\theta)) + P_4(\cos(\theta))$ function. The presence of the P_4 term would imply in the independent-particle model that in Eq. (1) a and a' could not have the same value of $\frac{3}{2}$, because of the $|a-a'| \leq 4 \leq a+a'$ angular momentum conservation. In other words, the vacancy state is not in a pure $\frac{3}{2}$ angular momentum state, but there is a certain admixture of states with $\frac{5}{2}$ or larger angular momentum value. In the dipole-allowed transitions there was no indication of a P_4 term, but there it would be about 10^{-4} times smaller because of the strong dipole selection rule $\Delta(L,L'k)$.

The possibility that the detector response function (tail) was time dependent over the course of the measurement, thus producing a small variation in the pattern of a P_4 term, cannot be entirely excluded. For this reason the spectra were refitted with variable tail parameters but with fixed Lorentzian values. The quality of the fit was the same for the Ll–$L\alpha$ range. For the $L\beta$ complex it reduced the χ^2 value and the residuals by a factor of 2; however, it did not give clear evidence of better representation, since in the fit the Lorentzian values of the $L\beta_{3,4}$ lines were assumed to be the reported values [27], and for the L_3-O,P transitions the same value was assumed. Especially the $L\beta_{3,4}$ intensity ratios and Lorentzian widths have considerable scatter in the literature. If these model assumptions are not correct, the tail parameters may in part act to compensate the deviation. In addition it was found that we could not use the outer-shell binding energies from Ref. [28] for the fit. When the energies of these x rays were left as variables of the fit, the resulting values differed from Ref. [28], although they were dependent on the assumed tail and Lorentzian widths. Nevertheless they were close to the more recent values reported by [29]. The results of this fit gave the same angular distributions for the dipole-allowed transitions; even the individual ratios were not altered at any angle. This is not surprising as the total tail area is less than 0.5% of the peak area. Although the Ls line intensity is 0.07% of the $L\alpha$ peak, the tail area under the Ls peak area is of the order of 20% of the Ls peak intensity, and at that level the change in the tail parameters will affect the calculated peak area. It is obvious that the tail parameters will modify the Ls line intensity, but they can only modify the Lt intensity through modifying the background, or the Lorentzian tail by modifying the Lorentzian widths. Fitting the spectra in this way (variable tail as opposed to average tail) gave the same results for the Ls and Lt anisotropy in each of the 2 and the 3 MeV measurements, and together with the 1 MeV measurement they are presented in Fig. 6. However, for the 1 MeV measurement this fit resulted in a smaller P_4 term Fig. 5(b) with much of the P_4 dependence accounted for in an angular dependent tail area, Fig. 5(c).

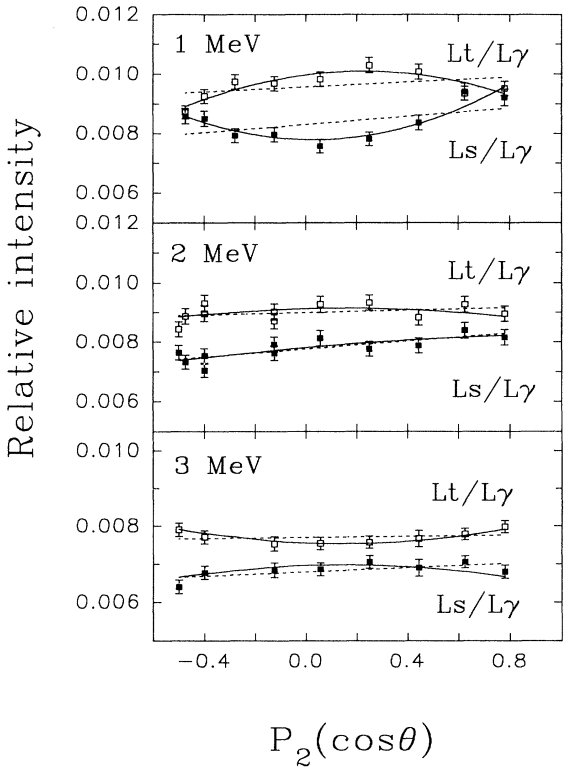

FIG. 6. Angular distributions of the dipole-forbidden Lt and Ls transitions of thorium ionized by 1-, 2-, and 3-MeV protons, and normalized to the intensity of the $L\gamma$ group x rays. The dashed lines are the best fit by second-order Legendre polynomial, while the full curves represent the fit by second- and fourth-order Legendre polynomial.

The possible origin of this angular distribution in the tail area is not clear to us, since the scattering chamber is cylindrically symmetric around the axis perpendicular to the observation plane, except for the small area openings for the beam entrance and the x-ray exits. If it has an origin in some scattering process of x rays, we would expect the same angle dependence at every proton energy. However, it was not observed in the 2 and 3 MeV measurements. The radiative Auger transitions have low transition probability for this subshell. We did not find any angular distribution formula for the radiative Auger transitions in the literature, and we did not attempt to calculate it. In our case the outgoing Auger electron is not observed, and this corresponds to the "stretched" angular momentum case [30]. If this P_4 dependence has an origin in the radiative Auger process it should show up at other proton energies, and should have the same energy dependence as the alignment parameter, but again it was not visible in the data. As an additional test we analyzed the Ll range including the radiative Auger transitions at the associated energies, and again the intensities obtained cannot explain this angular distribution.

The possibility of time-dependent detector response being the cause of this effect was pursued further, through an analysis of the M-shell x rays, which are present in all

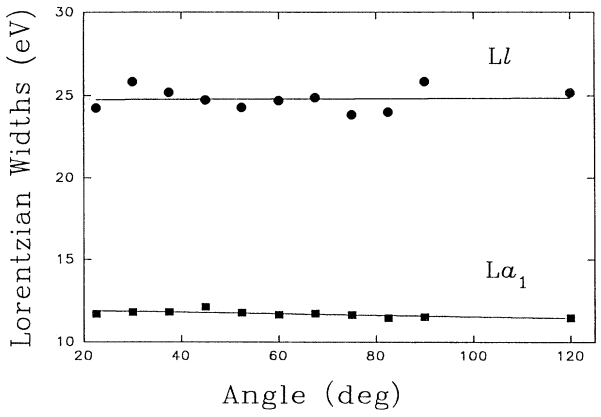

FIG. 7. Lorentzian widths of the Ll and $L\alpha_1$ transitions of thorium as a function of the observation angle for 1-MeV proton impact.

our L x-ray spectra. We fitted the M x-ray region and extracted the intensities of the $M\alpha$, $M\beta$, and $M\gamma$ groups and the corresponding silicon escape peaks. The intensity ratios of each escape peak to its parent were found to be constant, showing no trends with detector angle. Fitting these data with the function (2) gave a value of -0.0054 ± 0.014 for the anistropy parameter β_2. When a P_4 term was included in the fit, the resulting coefficients were $\beta_2=-0.0055\pm0.015$ and $\beta_4=-0.0005\pm0.01$. There is thus no evidence from the escape peak ratios of any changes in the dead layer characteristics that would cause the detector response function to alter. The uniformity of the escape peak ratios and their lack of anisotropy thus provide an additional indication that the P_4 term does not arise from time dependence of the response function.

As a final check we repeated the fit for the Ll and $L\alpha$ range, letting the Lorentzian widths, line intensities, and tail parameters be variables of the fit. The $L\alpha_2$ width was fixed relative to the $L\alpha_1$ width assuming the same ratio as was reported in Ref. [31]. In Fig. 7 the Lorentzian widths are plotted as a function of the angle and, as is shown, the widths were not affected by the variation in tail parameters. The remarkably small scattering of the Lorentzian widths indicates the reliability of the fit, and the accuracy of the data reported in Ref. [11]. It also shows that the Lorentzian broadening is important for the determination of peak areas, especially when angular distributions are studied, since the underlying Lorentzian tail has the same angular distribution as the peak to which it belongs.

IV. RESULTS AND DISCUSSION

The angular distributions of the analyzed transitions are presented in Fig. 4 for the Ll, $L\alpha_2$, and $L\alpha_1$ transitions, and the parameters of the fitted angular distributions are listed in Table II. For the 1-MeV data we performed various fits: neglecting tailing completely, using various tail functions, variable Lorentzian widths, etc. From this study we determined the dependence of the anisotropy parameters on the assumed model, in order to estimate the systematic errors in data evaluation. These errors are shown in parenthesis and we consider them as upper limits for the systematic error.

The first important piece of information is the angular distribution of the L_2 transitions normalized to the $L\gamma$ group. The $L\eta$ (L_2M_1) transition has a special character in that both the initial and final state are $\frac{1}{2}$ angular momentum states, which excludes the possibility of any alignment effect on the initial or final states. This transition would thus give a direct measure of any anisotropy of the $L\gamma$ group. Additionally it is located on the pronounced tail of the $L\beta_{2,15}$ and $L\beta_6$ transitions, which have large anisotropy. If part of that tail area had been included in this peak it would have shown up in the angular distribution, but this was not the case, as the normalized peak intensity ratio was found to be isotropic at every projectile energy. Similarly the $L\beta_1$ peak which originates from the filling of the L_2 subshell vacancy by an M_4 subshell electron was found to be isotropic at all energies. This transition is a very intense one, which is little affected by the fitting methods. It can serve as the measure of any alignment effect on the M_4 shell, if there is a simultaneous ionization in this shell. Such an effect was not found, in accordance with the theoretical expectations [6,32]. The $L\beta_1/L\gamma$ and the $L\beta_1/L\eta$ intensity ratios were found to be isotropic. Since the $L\alpha_2$ transition is filled from the M_4 subshell this transition would be affected in the same manner.

The principal aim of the present study was to deter-

TABLE II. Anisotropy parameters [β_2, Eq. (3)] for the relative x-ray yields of various L-shell transitions for proton impact on thorium. The systematic errors are shown in parentheses.

	β_2		
Transition	1 MeV	2 MeV	3 MeV
$Ll/L\gamma$	-0.138 ± 0.007 (±0.002)	-0.0956 ± 0.0043	-0.0288 ± 0.0020
$L\alpha_2/L\gamma$	0.156 ± 0.002 (±0.005)	0.0814 ± 0.0047	0.0289 ± 0.0035
$L\alpha_1/L\gamma$	-0.0377 ± 0.0022 (±0.002)	-0.0244 ± 0.0019	-0.0067 ± 0.0018
$L\alpha_{1,2}/L\gamma$	-0.0190 ± 0.0016 (±0.001)	-0.0154 ± 0.0016	-0.0032 ± 0.0019
$L\eta/L\gamma$	-0.0065 ± 0.0064	-0.0028 ± 0.0041	0.0029 ± 0.0062
$L\beta_6/L\gamma$	-0.1407 ± 0.0066	-0.0825 ± 0.0050	-0.0301 ± 0.0026
$L\beta_{2,15}/L\gamma$	-0.024 ± 0.003	-0.0145 ± 0.0014	-0.022 ± 0.017
$L\beta_1/L\gamma$	0.004 ± 0.015	0.008 ± 0.014	0.009 ± 0.013

mine the angular distribution of the $E1$-forbidden transitions and to probe the consistency between anisotropy parameters of $E1$-allowed transitions. For this reason we did not derive alignment parameters to compare with ionization theories. In the single-particle model the ratios of the anisotropy parameters are equal to the ratios of the α parameters [Eq. (6)]. These ratios are presented in Table III, with the single-particle model ratios [7,8,16], calculated using the multipole mixing parameters of the RHF calculation [7]. Any disagreement between the experimental and the theoretical values may come from the invalidity of the single-particle model or from the mixing ratios. Since these ratios characterize the decaying atoms only, at first sight it might be thought that these ratios should be independent of the ionizing proton energies. This idea governed our earlier studies [6,9], where we carried out measurements at only one projectile energy, chosen to provide the maximum alignment value ($A_2 \approx -0.5$). This value is accidentally the same as the A_2 value of the L_3 subshell in K-L angular correlations. Since the components of the alignment tensor are proportional to the spherical components of the electric quadrupole tensor [14], when there is a large alignment there will be a large deviation from the spherically symmetric potential. This deviation will depend on the proton energy through the energy dependence of the alignment tensors. Similar mixing of the atomic state might then be expected as was found in the case of anisotropic angular correlations between K x rays and γ rays caused by nuclear quadrupole deformations [33,34]. Theoretical calculations for the angular distributions using the two potential formalisms similar to [3] but allowing directional wave functions as used in Ref. [35] would be necessary to describe this type of mixing. Indeed the $2p_{3/2}$ wave function has strong directional dependence. If we assume $A_2 = -0.5$, which is near the value of the alignment at 1-MeV proton impact, using the equation of $A_{20} = [\sigma(\frac{3}{2},\frac{3}{2}) - \sigma(\frac{3}{2},\frac{1}{2})]/[\sigma(\frac{3}{2},\frac{3}{2}) + \sigma(\frac{3}{2},\frac{1}{2})]$ we calculate that the $j=\frac{3}{2}$, $m=\frac{1}{2}$ state has an ionization cross section [denoted by $\sigma(\frac{3}{2},\frac{1}{2})$] 3 times larger than the $j=\frac{3}{2}$, $m=\frac{3}{2}$ state. The largest effect would have been on the $3s_{1/2}$ state since there is a strong correlation between the $2p_{3/2}$ and $3s_{1/2}$ states [19]. In this case Eq. (3) may not be valid, and one may need a more complicated expression, which can be approximated in first order as

$$\beta_k = c\alpha_k(A_k)A_k \ . \tag{7}$$

Since the ionization and decaying processes can be treated independently, the separation of the A_k term is justified. We think from this simple model, which needs confirmation or otherwise from theoretical calculations that the energy dependence of the anisotropy parameter ratios cannot be excluded.

Although the size of the energy dependence of the anisotropy parameter ratios is comparable with the error bars in some cases, it suggests an energy-dependent trend. Using our sophisticated spectrum fitting technique, and taking advantage of the good resolution Si(Li) detector, with high counting statistics, we believe that the anisotropy parameters are reliable for the well-separated transitions such as Ll, $L\alpha_{1,2}$, $L\beta_6$, normalized to the $L\gamma$ group. At the outset we did not expect similarly reliable data for the $L\alpha_2$ transition since it is unresolved from the $L\alpha_1$ line, which is an order of magnitude more intense; however, the analysis proved otherwise. The $L\alpha_2$ and $L\alpha_1$ line intensity ratio determined from the angular distribution fit [the ratio of W_0 from Eq. (2)] was 0.112 ± 0.02; this value was independent of the proton energy and was in good agreement with the theoretical value of Scofield, which is 0.114. The angular distribution was extremely well described with the $P_2(\cos(\theta))$ function (Fig. 4). Additionally the Lorentzian widths were constant at every angle, and the scatter of the experimental points was very small (Fig. 7). The most reliable data are expected at 1-MeV proton energy, where the anisotropy is large. At 3 MeV the transitions are almost isotropic and as a consequence the ratios of anisotropy parameters bear large error bars. The angular distribution of the Lt and Ls transitions are presented in Figs. 5 and 6 and in Table IV, where the first row at every transition has the parameters of the fit by zero and second order, while the second row has the parameter values by zero, second and fourth-order Legendre polynomials. At 1 MeV both fitting methods result in a P_4 term that is larger than one-standard-deviation error for the Lt transition. At 3 MeV the presence of the P_4 term is pronounced. The β_4 parameter has a monotonic dependence as a function of the proton energy, as does the alignment parameter. The presence of the P_4 term is not expected on the basis of the independent-particle model, as was discussed earlier in the data evaluation section.

To make a comparison, we calculated the transition probabilities with the computer code GRASP [36], assuming closed outermost shells and single configurations; this was done using a RISK6000 computer. The following values were obtained for the mixing ratios in Coulomb gauge: $|\delta(Lt{:}M1/E2)| = 0.233$, $|\delta(Ls{:}M1/E2)| = 0.128$,

TABLE III. Anisotropy parameter ratios of various relative x-ray transition yields of the L_3 subshell of thorium. The theoretical values were obtained from Ref. [7].

β_2 ratios	1 MeV	2 MeV	3 MeV	Theoretical
$Ll/L\alpha_{1,2}$	7.27±0.69	6.22±0.70	5.07±1.31	7.74
$L\beta_6/L\alpha_{1,2}$	7.41±0.69	5.37±0.66	5.26±1.39	7.65
$Ll/L\alpha_2$	−0.88±0.04	−1.17±0.08	−1.04±0.14	−1.208
$L\alpha_1/L\alpha_2$	−0.242±0.013	−0.299±0.029	−0.24±0.07	−0.286
$L\beta_6/L\alpha_2$	−0.90±0.034	−1.013±0.085	−1.075±0.157	−1.193
$Ll/L\alpha_1$	3.66±0.29	3.80±0.43	4.31±1.12	4.217

TABLE IV. Coefficients of the angular distribution fits for the electric-dipole-forbidden transitions of thorium ionized by proton impact. The first row at every transition has the parameters of the fit by zero and second order, while the second row has the parameter values by zeroth-, second- and fourth-order Legendre polynomials. The individual spectra were fitted by two methods: (i) using average tail parameters for Si(Li) detector response function (see text), (ii) allowing variable tail parameters for the fit. In the 2- and 3-MeV cases, the two methods gave the same results.

Energy	Transition	β_2	β_4	χ^2_ν
1 MeV	$Lt/L\gamma$	0.057±0.037		4.2
Average tail		0.041±0.021	−0.131±0.031	1.10
	$Ls/L\gamma$	0.083±0.055		5.6
		0.085±0.027	0.192±0.041	1.25
	$L\beta_{9,10}/L\gamma$	0.0177±0.0261		9.5
		0.0173±0.012	−0.097±0.019	1.831
1 MeV	$Lt/L\gamma$	0.070±0.022		1.21
Variable tail		0.067±0.016	−0.043±0.025	0.96
	$Ls/L\gamma$	0.085±0.013		0.4
		0.084±0.014	−0.016±0.022	0.45
	$L\beta_{9,10}/L\gamma$	0.025±0.026		5.8
		0.014±0.027	−0.033±0.042	4.6
2 MeV	$Lt/L\gamma$	0.023±0.032		1.135
		−0.021±0.021	−0.041±0.032	1.06
	$Ls/L\gamma$	0.047±0.022		1.06
		0.064±0.023	−0.018±0.034	1.16
	$L\beta_{9,10}/L\gamma$	−0.004±0.010		1.22
		−0.0011±0.020	−0.039±0.031	1.05
3 MeV	$Lt/L\gamma$	0.012±0.020		1.85
		0.016±0.005	0.069±0.007	1.28
	$Ls/L\gamma$	0.029±0.030		1.76
		0.040±0.014	−0.0522±0.020	1.36
	$L\beta_{9,10}/L\gamma$	−0.008±0.012		1.32
		−0.006±0.018	0.025±0.026	1.51

$|\delta(Ls{:}M3/E2)|=0.0155$. Using these values we calculated the α parameters for these transitions using Eq. (6), as $\alpha(Lt)=-0.098$, $\alpha(Ls)=-0.2207$. The β_2 anisotropy parameters are in a good agreement with the ones obtained from theoretical calculations, if the alignment parameters are determined from the $L\alpha_2$ transitions.

V. CONCLUSIONS

Similar to earlier studies [9,11,37] the present analysis shows that the anisotropy of various $E1$-allowed transitions deviates from the theoretical calculations carried out using the independent-particle model. The ratios of the anisotropy parameters are expected to be independent of the ionization process; however, they showed a dependence on the proton energy. This energy dependence cannot be explained by the presence of higher-order multipole transitions. Rather, its description may require the use of more complex wave function which reflects the directional properties (alignment) of the ionized atoms.

An attempt was made to determine the angular distribution of the $E1$-forbidden Lt and Ls transitions. The β_2 anisotropy parameters are in good agreement with the ones obtained from theoretical calculations, if the alignment parameters are determined from the $L\alpha_2$ transition. However, the angular distributions contain in addition small fourth-order Legendre polynomial terms, an observation which contradicts the assumption that the ion with an aligned vacancy on the $2p_{3/2}$ subshell can be characterized as a pure angular momentum state.

If this P_4 term had arisen from anisotropies inherent in our experimental design, then similar contributions would be expected in the $E1$-allowed transitions from the same spectra. However, none of the $E1$ transitions showed such a trend. Nor was it present in the angular distribution of the nickel $K\alpha$ radiation which we used to test experimentally for cylindrical symmetry. The other obvious possible origin of the effect lay in a time-dependent detector tailing, but our experimental protocol and data analysis appear to preclude this.

The present measurements show the same disparity with theory for $E1$-allowed transitions as was found earlier. Presently available single-particle models exclude the variations in anisotropy parameter ratios for such transitions. Turning to the $E1$-forbidden transitions, the P_4 term is absent in nonrelativistic single-particle models; however, the question of whether all models exclude it is a complex one, and, as we indicated, relativistic effects

need to be better understood. We suggest that the next step might be to carry out measurements using polarized photons for excitation where the combination of the various mixings (e.g., $M2/E1$ or mixed angular momenta states) are different than in the cylindrically symmetric systems; many transitions will have large P_1 terms, which are very sensitive to the participating angular momenta. In addition, the components of the polarization tensor can also be determined. Also, it would be useful to make theoretical angular distribution calculations available with more refined wave functions [35,38].

ACKNOWLEDGMENTS

We would like to thank R. G. Gingerich and W. J. Teesdale for operating the Van de Graaff accelerator. We thank the Natural Sciences and Engineering Research Council of Canada for financial support.

*Permanent address: Institute of Nuclear Research of the Hungarian Academy of Sciences (ATOMKI), Debrecen, H-4001, Pf. 51, Hungary.

[1] M. H. Chen, in *Proceedings of the Fifteenth International Conference on X-Ray and Inner-Shell Ionization,* edited by T. A. Carlson, M. O. Krause, and S. T. Manson, American Institute of Physics Conf. Proc. No. 215 (AIP, New York, 1990), pp. 391–407.
[2] J. L. Campbell, Nucl. Instrum. Methods Phys. Res., Sect. B **31**, 518 (1988).
[3] J. H. Scofield, Phys. Rev. A **10**, 1507 (1974).
[4] J. H. Scofield, in *Atomic Inner-Shell Processes,* edited by B. Crasemann (Academic, New York, 1975), p. 265.
[5] W. Jitschin, G. Materlik, U. Werner, and P. Funke, J. Phys. B **18**, 1139 (1985).
[6] T. Papp, and J. Pálinkás, Phys. Rev. A **38**, 2686 (1988); T. Papp, J. Pálinkás, and L. Sarkadi, *ibid.* **42**, 5452 (1990).
[7] J. H. Scofield, Lawrence Livermore Laboratory Report No. UCRL-51231, 1972 (unpublished); and (private communication).
[8] E. G. Berezhko and N. M. Kabachnik, J. Phys. B **10**, 2467 (1977).
[9] T. Papp, Y. Awaya, A. Hitachi, T. Kambara, Y. Kanai, T. Mizogawa, and I. Török, J. Phys. B **24**, 3797 (1991).
[10] J. L. Campbell and J. X. Wang, X-Ray Spectrom. **20**, 191 (1991).
[11] T. Papp, J. A. Maxwell, W. J. Teesdale, and J. L. Campbell, Phys. Rev. A **47**, 333 (1993).
[12] T. Papp, J. L. Campbell, J. A. Maxwell, J.-X. Wang, and W. J. Teesdale, Phys. Rev. A **45**, 1711 (1992).
[13] S. Devons and L. J. B. Goldfarb, in *Handbuch der Physics,* edited by S. Flugge (Springer, Berlin, 1957), Vol. 42, p. 362.
[14] K. Blum, *Density Matrix Theory and Applications* (Plenum, New York, 1981).
[15] A. J. Ferguson, *Angular Correlation Methods in Gamma-Ray Spectroscopy* (North-Holland, Amsterdam, 1965).
[16] H. J. Rose and D. M. Brink, Rev. Mod. Phys. **39**, 306 (1967).
[17] W. Jitschin, H. Kleinpoppen, R. Hippler, and H. O. Lutz, J. Phys. B **12**, 4077 (1979).
[18] L. Végh and R. L. Becker, Phys. Rev. A **46**, 2445 (1992).
[19] A. W. Weiss, in *Beam-Foil Spectroscopy,* edited by I. A. Sellin and D. J. Pegg (Plenum, New York, 1976).
[20] H. A. Bethe and E. E. Salpeter, *Quantum Mechanics of One and Two Electron Atoms* (Springer, Berlin, 1957).
[21] V. B. Berestetskii, E. M. Lifshitz, and L. P. Pitaevskii, *Quantum Electrodynamics,* 2nd ed. (Pergamon, Oxford, 1982), p. 168.
[22] P. Indelicato and E. Lindroth, Phys. Rev. A **46**, 2426 (1992); O. Gorceix, P. Indelicato, and J. P. Desclaux, J. Phys. B **20**, 639 (1987).
[23] T. Papp and J. L. Campbell, J. Phys. B **25**, 3765 (1992).
[24] W. Jitschin, R. Hippler, R. Shanker, H. Kleinpoppen, R. Schuch, and H. O. Lutz, J. Phys. B **16**, 1417 (1983).
[25] J. Pàlinkàs, L. Sarkadi, B. Schlenk, I. Török, Gy. Kàlmàn, C. Bauer, K. Brankoff, D. Grambole, C. Heiser, W. Rudolph, and H. J. Thomas, J. Phys. B **17**, 131 (1983).
[26] J. A. Maxwell, J. L. Campbell, and W. J. Teesdale, Nucl. Instrum. Methods Phys. Res., Sect. B **43**, 218 (1989).
[27] S. I. Salem and P. L. Lee, At. Data Nucl. Data Tables **18**, 234 (1976).
[28] J. A. Bearden, Rev. Mod. Phys. **39**, 78 (1967).
[29] G. M. Bancroft, T. K. Sham, and S. Larsson, Chem. Phys. Lett. **46**, 551 (1977).
[30] L. C. Biedenharn and J. D. Louck, in *Angular Momentum in Quantum Mechanics,* Encyclopedia of Mathematics and Its Applications, edited by G.-C. Rota (Addison-Wesley, Reading, MA, 1981), Vol. 8.
[31] M. H. Chen, B. Crasemann, and H. Mark, Phys. Rev. A **21**, 449 (1980); **27**, 2989 (1983).
[32] T. Papp and L. Kocbach, J. Phys. (Paris) Colloq. **48**, C9-243 (1987).
[33] A. E. Khalil, Phys. Rev. C **28**, 2414 (1983).
[34] S. K. Sen, D. L. Salie, and E. Tomchuk, Phys. Rev. Lett. **28**, 1295 (1972).
[35] Y. K. Kim, Phys. Rev. **154**, 17 (1967).
[36] K. G. Dyall, I. P. Grant, C. T. Johnson, F. A. Parpia, and E. P. Plummer, Comput. Phys. Commun. **55**, 425 (1989).
[37] P. N. Johnston, Phys. Rev. C **44**, R586 (1991).
[38] M. Ohno and R. E. LaVilla, Phys. Rev. A **45**, 4713 (1992).